Oncogene
https://doi.org/10.1038/s41388-019-0782-x

ARTICLE

Hypoxia-induced tumor exosomes promote M2-like macrophage polarization of infiltrating myeloid cells and microRNA-mediated metabolic shift

Jung Eun Park[1] · Bamaprasad Dutta[1] · Shun Wilford Tse[1] · Nikhil Gupta[1] · Chee Fan Tan[1] · Jee Keem Low[2] · Kheng Wei Yeoh[3] · Oi Lian Kon[4] · James P. Tam[1] · Siu Kwan Sze[1]

Received: 11 August 2018 / Revised: 8 February 2019 / Accepted: 4 March 2019

Abstract

Developing tumors rapidly outgrow their oxygen supply and are subject to hypoxia, which stimulates hypersecretion of tumor-derived exosomes that promote angiogenesis, metastasis, and immunosuppression, but the molecular mediators of these pathological effects remain poorly defined. Using quantitative proteomics, we identified that exosomes produced by hypoxic tumor cells are highly enriched in immunomodulatory proteins and chemokines including CSF-1, CCL2, FTH, FTL, and TGFβ. Modeling exosome effects on tumor-infiltrating immune cells, we observed a potent ability of these hypoxia-induced vesicles to influence macrophage recruitment and promote M2-like polarization both in vitro and in vivo. In addition, hypoxic, but not normoxic, tumor exosomes enhanced oxidative phosphorylation in bone marrow-derived macrophages via transfer of let-7a miRNA, resulting in suppression of the insulin-Akt-mTOR signaling pathway. Together, these data demonstrate that hypoxia promotes tumor secretion of biomolecule-loaded exosomes that can modify the immunometabolic profile of infiltrating monocyte-macrophages to better evade host immunity and enhance tumor progression.

Introduction

Low oxygen availability or 'hypoxia' stress in developing tumors stimulates secretion of small, membrane-bound vesicles known as exosomes that can promote angiogenesis, metastasis, and suppression of host immunity to drive disease progression [1, 2]. While exosomes can mediate steady-state communication between cells and the microenvironment in healthy tissues [3], their ability to deliver proteins, DNA, and RNAs to host leukocytes has also been strongly implicated in several key pathological processes [4, 5]. It is now clear that exosomal transfer of bioactive molecules allows tumors to influence the behavior of infiltrating immune cells, but the molecular mediators and mechanisms by which the exosomal cargo supports disease progression remain poorly defined.

An essential role of exosomes in tumorigenesis has already been demonstrated in breast cancer, gastric cancer, and melanoma [6–8]. However, the biomolecule cargo of these exosomes is highly diverse and can exert variable effects on tumor angiogenesis, cell migration, and priming of the pre-metastatic niche via interactions with healthy stromal tissues [6, 9, 10]. Some researchers have reported that tumor exosomes are immunogenic and elicit specific host responses that might influence disease outcome. For example, tumor antigen-loaded vesicles derived from dendritic cells and macrophages have been shown to exhibit T-cell stimulatory activity mediated by transfer of MHC I/II,

Supplementary information The online version of this article (https://doi.org/10.1038/s41388-019-0782-x) contains supplementary material, which is available to authorized users.

✉ Jung Eun Park
jepark@ntu.edu.sg

✉ Siu Kwan Sze
sksze@ntu.edu.sg

[1] School of Biological Sciences, Nanyang Technological University, 60 Nanyang Drive, Singapore 637551, Singapore

[2] Department of Surgery, Tan Tock Seng Hospital, 11 Jalan Tan Tock Seng, Singapore 308433, Singapore

[3] National Cancer Centre Singapore, Department of Radiation Oncology, 11 Hospital Drive, Singapore 169610, Singapore

[4] National Cancer Centre Singapore, Division of Medical Sciences, 11 Hospital Drive, Singapore 169610, Singapore

Published online: 12 March 2019

CD54, CD80, and CD86 [11, 12]. Similarly, exosomes isolated from primary human body fluids have been observed to activate monocytic cells via toll-like receptor signaling [13]. However, the majority of prior studies have reported that tumor-derived exosomes are typically immunosuppressive [14]. In leukemia, tumor exosomes exhibit membrane-bound TGF-β1 and disrupt NK cell activity to mediate immune evasion [15, 16], while in gastric cancer and melanoma, exosomes display variable lymph node localization and disease-enhancing effects depending on their source [7, 10, 17]. Taken together, these data indicate that tumor exosomes can exert potent effects on host immunity and are likely to represent key determinants of the clinical course in human cancer.

Numerous studies have investigated the role of tumor-derived exosomes in cancer progression, but little is known about how the tumor microenvironment alters the content of exosome vehicle and the consequence of these alterations in the context of immune response. Since microenvironmental stress is already known to modulate exosomal sorting mechanisms in healthy cells and tissues [18, 19], we hypothesized that low oxygen availability also modifies the molecular composition of tumor exosomes. Indeed, given that hypoxia is recognized as a key regulator of tumor progression, it is likely that exosomes secreted by hypoxic cancer cells exhibit immunomodulatory effects and induce microenvironmental changes to support tumor development [1, 20]. In the current report, we identify a potent ability of hypoxic tumor exosomes to promote M2-like polarization of infiltrating macrophages driven by microRNA (miRNA)-mediated induction of an oxidative phosphorylation (OXPHOS) metabolic profile that favors tumor development.

Results

Hypoxia enhances tumor secretion of exosomes enriched in immunosuppressive proteins

To explore the immunological effects of tumor exosomes secreted under hypoxic conditions, we exposed mouse melanoma B16-F0 cells to normoxia (21% O_2) or hypoxia (<0.5% O_2) for 24 h in a hollow fiber cell culture system that generates a 3D environment to mimic conditions in vivo [21]. Exosomes isolated from the cell culture supernatants were then subjected to tandem mass tags (TMT)-based quantitative proteomic analysis as described in the Materials and Methods and shown in Fig. 1a [22]. Nanoparticle tracking analysis of the isolated exosomes revealed an average diameter of 136 ± 42 nm, consistent with the 30−150 nm size range expected for these vesicles (Fig. 1b, Supplementary Videos 1 and 2), while western blot analysis confirmed the presence of characteristic exosomal markers Alix, CD63, and TSG101 (Fig. 1c). Exosome size distribution did not differ between normoxia and hypoxia conditions, but total exosomal proteins per cells were 3–4-fold higher under low-oxygen conditions in four cancer cell lines (Fig. 1d). Similar data were also obtained when assessing the impact of hypoxia on exosome secretion by nanoparticle tracking system in four cancer cell lines (Supplementary Fig. S1), thus indicating that oxygen restriction exerts potent effects on exosome loading across multiple tumor types. We next proceeded to identify and quantitate the exosomal proteins obtained using Mascot database search software (specific search criteria are described in the Materials and Methods). A total of 3710 proteins were identified based on at least two unique tryptic peptides and protein score ≥65 ($p < 0.05$; Supplementary Tables S1 and S2). Enrichment ratio was calculated as protein abundance in hypoxic exosomes relative to normoxic exosomes ($\log_2$ fold change ≤−1 and ≥1 were assigned as cut-off values based on volcano plot analysis; Fig. 1e, Supplementary Fig. S2). Using this approach, we observed that a total of 990 proteins (26.7% of total exosomal proteins) were at least 2-fold enriched in hypoxic exosomes, whereas only 220 proteins (5.9% of total) were more abundant in normoxic exosomes.

Microenvironmental hypoxia was associated with tumor exosome enrichment in several proteins already implicated in tumor–tumor or tumor–stroma interactions including chemokines, growth factors, pro-tumorigenic molecules, and various soluble inhibitory factors (Fig. 2a–d and Supplementary Table S3). Key components of these vesicles included the chemokines/chemoattractants macrophage colony-stimulating factor 1 (CSF-1), monocyte chemoattractant protein-1/C–C motif chemokine 2 (MCP-1/CCL2), endothelial monocyte-activating polypeptide 2 (EMAP2/AIMP1), and leukotriene A-4 hydrolase (LTA4H). We also observed marked exosomal enrichment in immunosuppressive mediators including transforming growth factor beta 1 (TGFβ1), TGFβ2, TGFβ3, macrophage migration inhibitory factor (MIF), and ferritin heavy/light chain (FTH, FTL). In addition, hypoxic tumor exosomes were further loaded with proteins that might contribute to tumor progression/metastasis and miRNA processing including matrix metalloproteinases 2 and 19, annexin A4 (ANXA4) and ANXA6, procollagen-lysine,2-oxoglutarate 5-dioxygenase 1 (PLOD1), PLOD2, argonaute 1 (AGO1), AGO3, and AGO4. In Table 1, we have summarized the roles of these enriched proteins in hypoxic exosomes. Key proteins enriched in hypoxic exosomes were further confirmed by western blot analysis in various cancer cell lines. As shown in Fig. 2e and Supplementary Fig. S2, the expression levels of CSF-1, FTH, or FTL were increased in hypoxic exosomes, which were isolated from B16-F0, A375, A431, and A549 lung adenocarcinoma cells.

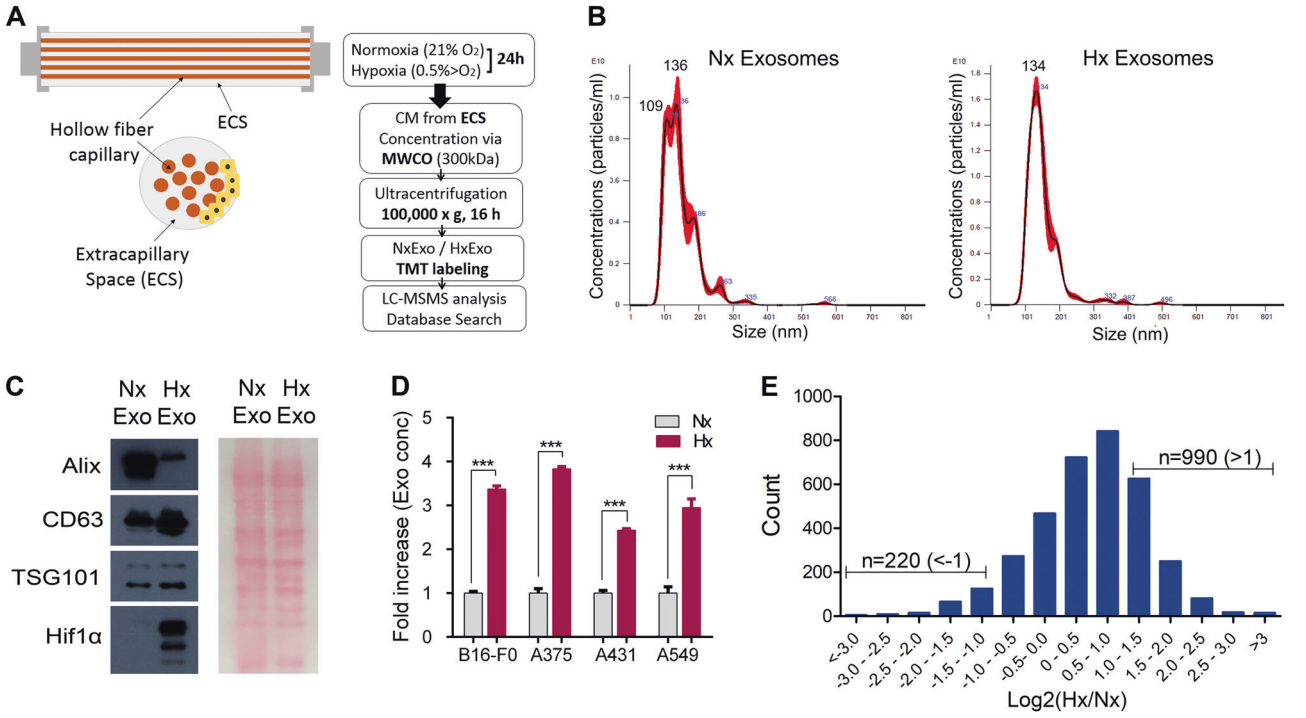

Fig. 1 Schematic diagram of hollow fiber cell culture system and proteomic workflow. **a** Schematic diagram of hollow fiber cell culture system and workflow of exosome extraction for proteomic analysis. **b** Nanoparticle tracking analysis of exosomes isolated from the extracapillary space (ECS) indicating mean diameter of 136 ± 42 nm. **c** Western blot analysis confirmed the presence of exosomal marker proteins, Alix, CD63, and TSG101. Ponceau staining was used as an equal loading control. **d** Comparison of total exosomal proteins secreted by normoxic cancer cells, B16-F0, A375, A431, A549, or their hypoxic counterparts. Data are displayed as mean ± SEM, ***$p < 0.0001$. **e** Histogram shows the distribution of fold-change in exosomal proteins comparing hypoxia with normoxia (Log_2 [Hx/Nx] ≤ −1 or ≥1 are indicated). NxExo normoxic exosomes, HxExo hypoxic exosomes

Previous studies have suggested that tumor-derived exosomes are loaded with immunosuppressive or pro-tumorigenic molecules [11, 14], but the exact role of exosomes released into the tumor microenvironment is still controversial. To further investigate the relation between tumor hypoxia and composition of the exosomal cargo, we analyzed protein co-expression level with the master regulator of hypoxia *HIF1α* and key exosomal proteins [23]. In order to do this, we used the computational gene co-expression search engine SEEK [24] to access publicly available microarray datasets, which revealed a close association of *HIF1α* with expression of target genes including *CCL2, CSF1, TGFβ2, TGFβ3, FTH1, PLOD2, LGALS3*, and *MIF* (Fig. 2f), across multiple tumor types including glioblastoma, lung, melanoma, and pancreatic cancers (Supplementary Table S4). Of these hypoxia/*HIF1α*-responsive genes, CSF-1 and CCL2 are known to be key mediators of monocyte/macrophage recruitment into tumors and contribute to the establishment of a pro-tumorigenic microenvironment [25, 26], while TGFβ and FTH1 potently suppress host immunity via induction of regulatory T-cells (Tregs) [27, 28]. Coordinated dispersal of these proteins via exosome release during tumor hypoxia is therefore likely to promote immune evasion and disease progression.

Hypoxic tumor exosomes promote M2-like polarization of infiltrating monocyte-macrophages

Our proteomics data revealed that hypoxic exosomes were highly enriched in potent chemoattractants for monocyte/macrophages (CSF-1, CCL2, and EMAP2), which can undergo differentiation into tumor-associated macrophages (TAMs) in the tumor microenvironment and promote cancer progression [29, 30]. We therefore assessed whether hypoxic tumor exosomes are capable of altering leukocyte recruitment by assessing their impact on cell motility in a standard Boyden chamber assay [31]. Macrophage-like RAW 264.7 cells exhibited 2- to 5-fold greater chemotactic responses to exosome-containing media than to PBS-only control medium (Fig. 3a) and cell migration was significantly enhanced when the bottom chamber contained exosomes from hypoxic tumors (4.3-fold, $p < 0.0001$). These data suggested that hypoxic tumors exhibit greater capacity to recruit monocyte/macrophages via exosome release into the local microenvironment. In order to assess this possibility in vivo, we next mixed B16-F0 tumor cells (1×10^6 cells) with normoxic exosomes, hypoxic exosomes, or matrigel-only control prior to subcutaneous (s.c.) injection to the backs of C57BL/6 mice ($n = 6$ animals per group). On day 14 after s.c. injection of

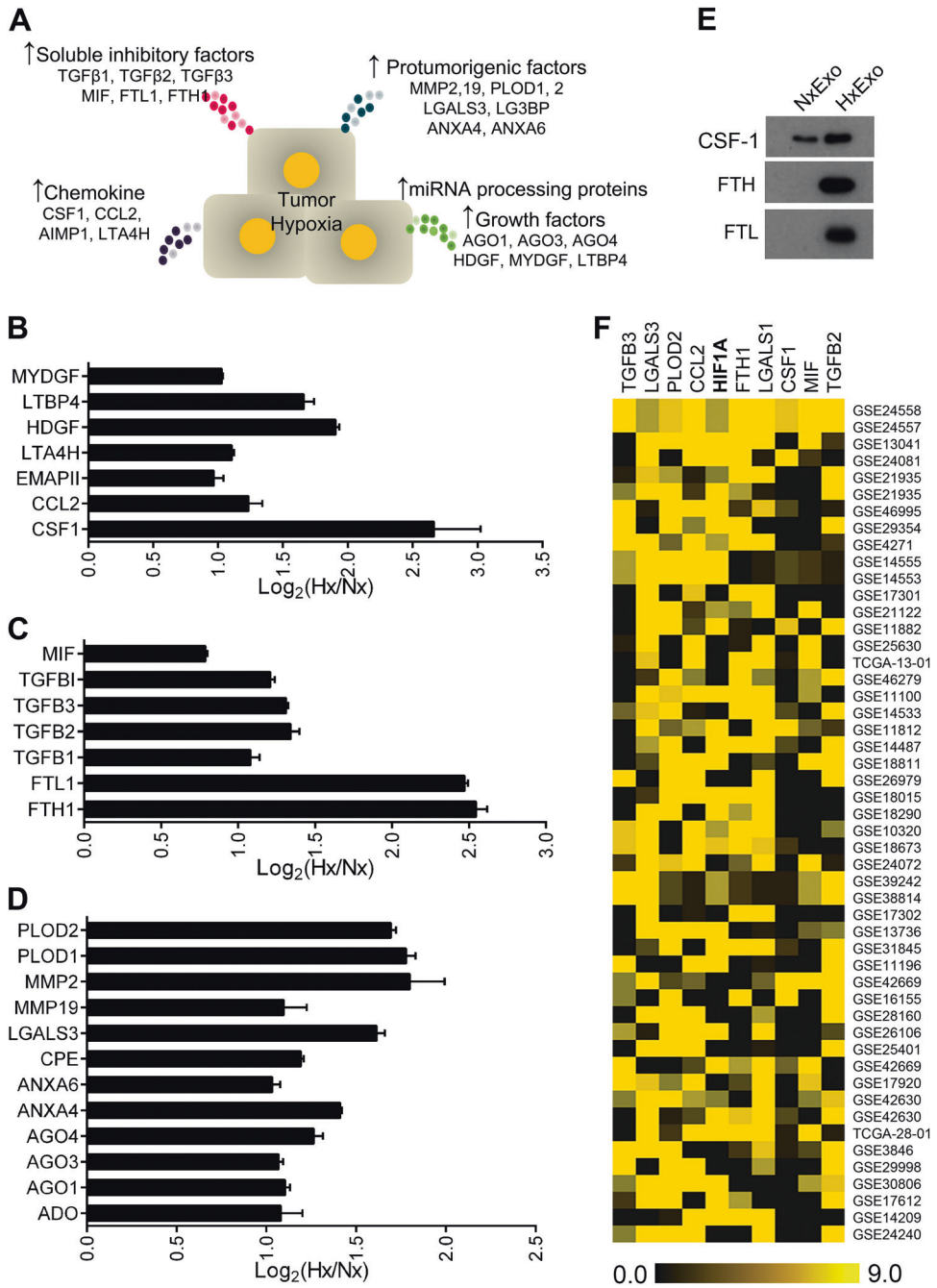

Fig. 2 Summary of exosomal proteins associated with immunosuppression and/or tumor progression. **a** Schematic overview of identified proteins that were enriched in exosomes released by hypoxic B16 melanoma cells. **b–d** Hypoxia-enriched exosomal proteins were classified into three main categories; **b** chemokines and growth factors, **c** soluble inhibitory proteins, and **d** pro-tumorigenic proteins and miRNA-processing proteins. Protein fold-changes are shown in log-scale. **e** Western blot analysis of key exosomal proteins, CSF-1, FTH, and FTL. **f** Analysis of *HIF-1α* co-expression with target genes *CCL2, CSF1, TGFβ2, TGFβ3, FTH1, PLOD2, LGALS2, LGALS3*, and *MIF* (as assessed using SEEK software)

B16-F0 cells, the mice were sacrificed and the tumor mass was isolated and dissociated for analysis by flow cytometry to evaluate M1- or M2-like macrophage recruitment/differentiation within the tumor area. As shown in Fig. 3b, tumor infiltration of F4/80^{+}CD206^{high} M2-like macrophage [32] was significantly increased by co-injection of hypoxic exosomes (fold change 3.93, $p = 0.0036$) compared to matrigel-only control, whereas only trace numbers of dendritic cells (CD11c^{hi}, lower right quadrant) or immunosuppressive Tregs (CD4^{+}CD25^{+}) were detected in the tumor region (Supplementary Fig. S3).

Since macrophages derived from myeloid precursor cells can exhibit pro-tumor or immunosuppressive activity upon CSF-1 or CCL2-mediated differentiation to M2-like macrophage or TAM in tumor local area, we further characterized the exosome-induced differentiation of myeloid cells using M2-like macrophage specific marker, CD206 [30]. Exosome-treated bone marrow-derived macrophages (BMMs) showed a shift of cell population to F4/80^{+}CD206^{high} population compared to control BMMs. Especially, hypoxic exosome promoted the expansion of F4/80^{+}CD206^{high} population by 1.74-fold compared to PBS control without IL-4 treatment,

Table 1 Role of the key exosomal proteins secreted from hypoxic cancer cells

Protein	Role in tumor/tumor microenvironment	Log_2(Hx/Nx) ratio	Refs.
CSF1	Monocyte/macrophage recruitmen Macrophage (TAM) differentiation Poor prognosis	2.663	[54–56]
CCL2	Monocyte/macrophage recruitment Cancer progression and metastasis	1.234	[57, 56]
EMAP2/AIMP1	Macrophage recruitment TAM accumulation	0.968	[58, 55]
LGALS3	M2 macrophage infiltration and angiogenesis in tumors	1.614	[59]
FTH	Immunosuppression, activation of regulatory T cell	2.545	[60, 61]
FTL	Immunosuppression, Tumor development, and prognostic biomarker	2.471	[62–64]
TGFβ 1 TGFβ 2 TGFβ 3	Immune evasion, cancer stemness, and metastasis	1.080 1.342 1.312	[65–67]
LTA4H	Chronic inflammation-associated carcinogenesis	1.104	[68, 69]
MIF	Immunosuppression, tumor development	0.788	[70, 71]
HDGF	Cancer cell invasion	1.905	[72]
MMP2 MMP19	Cancer progression	1.8 1.096	[73]
PLOD1	Tumorigenesis/cancer biomarker	1.778	[74]
PLOD2	Hypoxia-induced tumor metastasis	1.693	[75]
ANXA4	Tumor progression, invasion, metastasis, and drug resistance	1.412	[76]
AGO4 AGO3 AGO1	Processing of small RNA such as miRNA, siRNA for gene silencing	1.264 1.068 1.104	[77, 78]
ANXA6	Dual functions, acting as a tumor suppressor or promoter	1.033	[79, 80]

indicating a key role of tumor-derived exosome on M2-like macrophages induction (Fig. 3c). In addition, BMMs presented high $F4/80^{+}CD135^{high}$ phenotype, a hematopoietic stem cell marker, upon exosome treatment [33], implying the potential role of exosomes in stem cell development (Fig. 3d). IL-4 (20 ng/ml) was treated for M2-type macrophage polarization (Supplementary Fig. S4). Hypoxic exosome-mediated M2-like macrophage expansion was in line with BMMs cell growth. As shown in Fig. 3g, hypoxic exosome-treated BMMs showed 1.7-fold increase in cell number compared to M-CSF-only treated cells ($p = 0.0027$).

Given that macrophages can exhibit either anti-tumor (M1) or pro-tumor polarization (M2) upon cytokine-mediated activation of STAT1 or STAT6 signaling pathway, respectively [34, 35], we next sought to determine whether tumor exosomes can mediate this process by western blot analysis (Fig. 3e). While STAT1 phosphorylation was barely detected in either PBS- or exosome-treated BMMs, STAT6 phosphorylation was substantially increased in exosome-treated BMMs, consistent with an ability to promote M2-like polarization of tumor-infiltrating macrophages. Accordingly, expression of M2-like marker genes assessed by quantitative real-time PCR (RT-qPCR) showed that exposure to hypoxic exosomes for 48 h resulted in time-dependent upregulation of *Arg1* (arginase 1), *Ym1* (chitinase 3-like 3), and *Fizz1* (found in inflammatory zone 1) (Fig. 3f) [36].

To further explore the effects of cancer exosomes on M2-like macrophage polarization, exosomes were isolated from various cancer cell lines including A375, A431, and A549, and treated to THP-1 monocytic cells to test the expression of M2 markers. For this, THP-1 cells were treated with 20 ng/ml of PMA (Phorbol 12-myristate 13-acetate) for 24 h followed by resting in RPMI control media for 24 h to differentiate into M0-like macrophages. Once differentiated, M0-type THP-1 cells can be polarized to either M1- or M2-like macrophage response to different inducers [37]. Afterward, 5 μg/ml of cancer exosomes were treated to M0-type THP-1 cells for 48 h and applied to either FACS analysis or RT-qPCR analysis for M2-type markers such as the scavenging receptor CD163 or chemokine CCL13 [38, 39]. With PMA treatment, a clear increase in the level of CD163 was found in THP-1 cells, and hypoxic exosome treatment increased the CD163-positive population up to 55% (Supplementary Fig. 6A). In addition, the expression level of CCL13 was upregulated in hypoxic exosome-treated THP-1 cells (Supplementary Fig. 6B), which indicated that exosomes derived from different hypoxia cancer

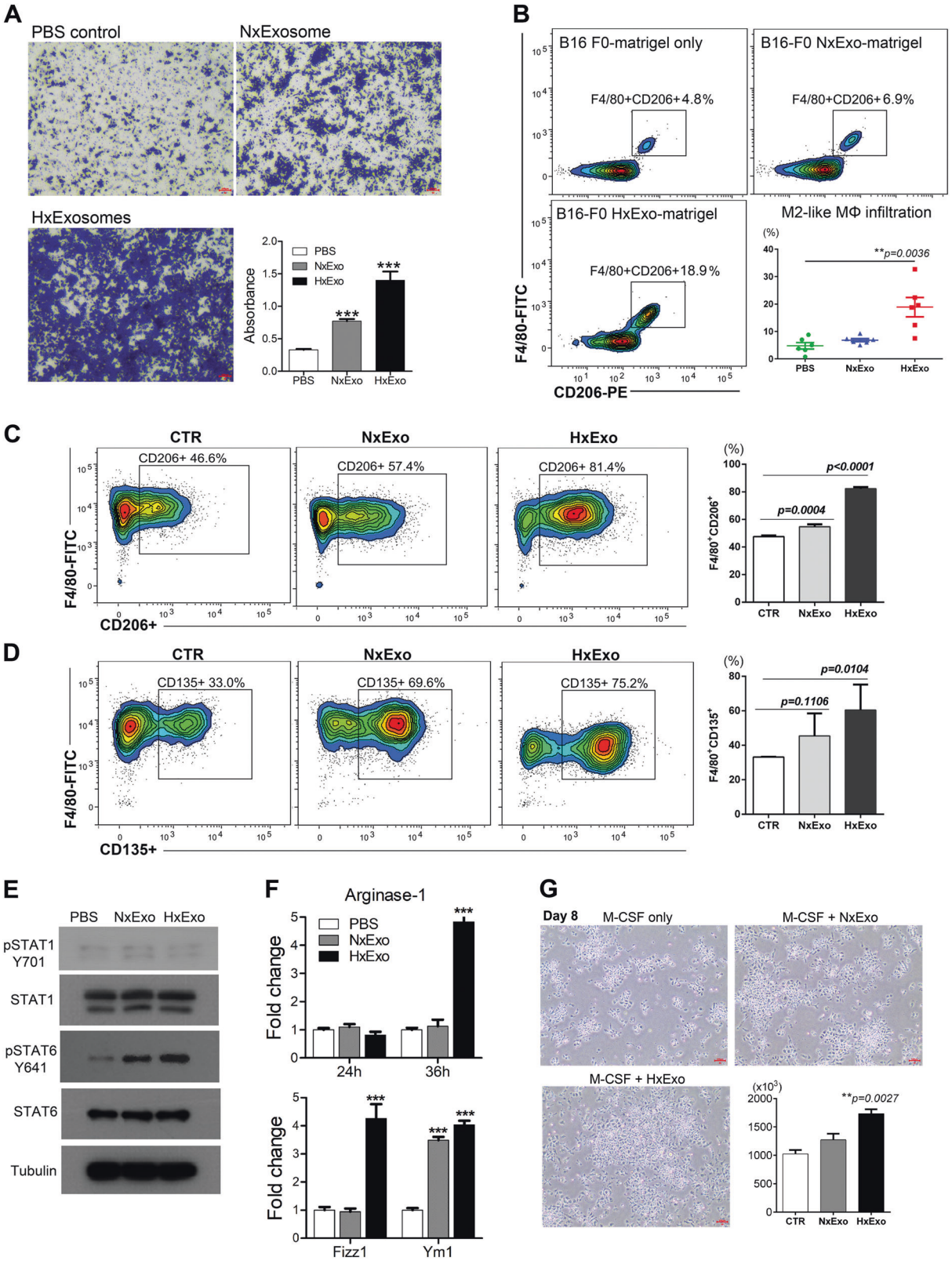

cell lines indeed contribute to M2-type macrophage polarization. Collectively, hypoxic tumor exosomes facilitate monocyte/macrophage recruitment both in vitro and in vivo, and drive protumoral M2-like macrophage polarization of the infiltrating cells to potentially enhance cancer development.

◀ **Fig. 3** Tumor-derived exosomes induce M2-like polarization of bone marrow-derived macrophages. **a** Macrophage-like RAW 264.7 cells were added to the Matrigel-coated upper wells of a Boyden chamber for assessment of chemotaxis toward normoxic or hypoxic exosomes added to the lower chamber. The cells were allowed to migrate for 24 h at 37 °C before staining with crystal violet and quantification. Data represent mean ± SEM of triplicate experiments, $***p < 0.0001$. **b** Immune cell infiltration analysis in tumor xenograft model. B16-F0 cells were pre-mixed with 50 µg of hypoxic or normoxic exosomes (or PBS-only control) prior to s.c. injection into C57BL/6 mice ($n = 6$ animals per group). On day 14, the resultant tumors were excised/dissociated and the phenotype/frequency of infiltrating Mφ was assessed by flow-cytometry. Representative dot-plots show $F4/80^{+}CD206^{high}$ phenotype in B16 tumors co-injected with PBS control, normoxic, or hypoxic exosomes. **c**–**f** Exosome-mediated M2-like polarization of BMMs. BMMs were co-cultured with 5 µg/ml of normoxic or hypoxic exosomes for 48 h and subsequently used for FACS analysis. PBS was used as a control group. **c** Data showed relative expression of $F4/80^{+}CD206^{high}$ on BMMs. **d** Data showed the relative expression of $F4/80^{+}CD135^{high}$ on BMMs. **e** Western blot analysis of STAT1, STAT6, p-STAT1 Y701, and p-STAT6 Y641 in exosome-treated macrophages. **f** RT-qPCR analysis of M2-like marker genes *Arg1*, *Fizz1*, and *Ym1*. Data represent mean ± SEM of triplicate experiments, $***p < 0.0001$. **g** Hypoxic tumor exosomes enhance the cell growth of BMMs. Bone marrow cells were cultured with M-CSF for 6 days to differentiate into BMMs and then treated with 5 µg/ml of NxExo or HxExo for 2 days. Trypan Blue dye exclusion test was used for viable cell counting. Hypoxic exosome treatment promoted cell growth of BMMs; $**p = 0.0027$

Hypoxic exosomes enhance mitochondrial OXPHOS in macrophages

M2-like macrophages have previously been reported to employ mitochondrial OXPHOS to sustain immune function, whereas M1-like macrophages and cancer cells use glycolysis to generate ATP [34, 40]. Metabolic reprogramming assists macrophages in adapting to their local microenvironment, thus shaping their activation state/effector functions and potentially impacting on disease progression. We therefore assessed whether exosome-mediated polarization of macrophages toward an M2-like profile was associated with changes in metabolic activity. We examined the metabolic shift in exosome-treated BMMs by measuring ATP-linked mitochondrial oxygen consumption rate (OCR) in response to oligomycin (OM), carbonyl cyanide-4-(trifluoromethoxy)-phenylhydrazone (FCCP), and rotenone (ROT) + antimycin A (AA). M2-like macrophages polarized by hypoxic exosomes exhibited enhanced OXPHOS activity at both basal respiration and ATP production level relative to cells treated with normoxic exosomes or PBS-only control (Fig. 4a, b), indicating that BMMs exposed to hypoxic exosomes undergo a metabolic shift toward TCA cycle activation and OXPHOS, which are archetypal characteristics of M2-like polarization [34]. We next assessed signaling pathways that might drive a metabolic shift from glycolysis to OXPHOS such as AKT-mTOR signaling pathway. Western blot analysis showed that hypoxic exosome-treated BMMs displayed reduction of AKT and mTOR phosphorylation while total AKT and mTOR were not affected and phosphorylation of p4E-BP and pS6K, direct substrates of mTOR activation, was subsequently reduced (Fig. 4c), together with increased expression levels of mTOR negative regulator REDD1 (Fig. 4d).

Exosomal let-7a miRNA regulates the mTOR signaling pathway in macrophages

Having observed that tumor-derived exosomes enhanced mitochondrial OXPHOS and suppressed mTOR activation in BMMs, we next sought to identify exosomal factors that might influence mTOR activity and/or glucose metabolism. Recently, miRNAs have emerged as key regulators of these signaling pathways to regulate cell metabolic process [41, 42], so we used RT-qPCR to assess the expression level of candidate miRNAs including let-7a and miR-21a in tumor-derived exosomes. Under hypoxic conditions, total let-7a miRNA expression in tumor cells was decreased to just ~30% of that detected in the normoxic control, whereas exosomal let-7a content was increased ~25-fold (Fig. 5a). These data indicate that let-7a miRNA is substantially decreased in hypoxic tumors via export from the cells mediated by exosome release. Exosomal miR-21a level was slightly increased in hypoxic exosomes (Supplementary Fig. S7). We therefore sought to explore the expression level of let-7a target genes in BMMs by RT-qPCR after exosome treatment. miRNA let-7a target genes, which involved in insulin signaling pathway, were predicted using TargetScan software (Fig. 5b) [43]. Using this approach, we observed that exposure to tumor exosomes significantly decreased the expression levels of let-7a target genes such as *IRS-1, IRS-2, INSR, and IGF1R* in BMMs (Fig. 5c). Consistent with these findings, when let-7a miRNA mimics was transfected into macrophage-like RAW 264.7 cells, we observed a significant decrease in the expression levels of *INS-1* and *IGF1R*, supporting that transfer of let-7a miRNA into target macrophages can mediate potent suppression of insulin signaling molecules (Fig. 5d). Since metabolic shift of immune cells affects the immune cell fate and function, we further analyzed key functional molecules in BMMs after exosome treatment. As shown in Fig. 6a, hypoxic exosome-treated BMMs displayed 30- to 80-fold higher expression of the TAM-associated genes *COX-2*, *PGES-1*, and *IL-6*, which have established roles in host immunosuppression and tumor growth. In contrast, normoxic tumor exosomes exerted only modest effects on macrophage expression of these genes (Fig. 6a). Interestingly, tumor-derived exosomes showed profound effect on BMMs but not on bone marrow-derived dendritic cells (BMDCs). Under the same treatment condition, BMDCs showed around 3–10-fold increase of *COX-2, PGES-1, IL-6* gene expression compared to control, but

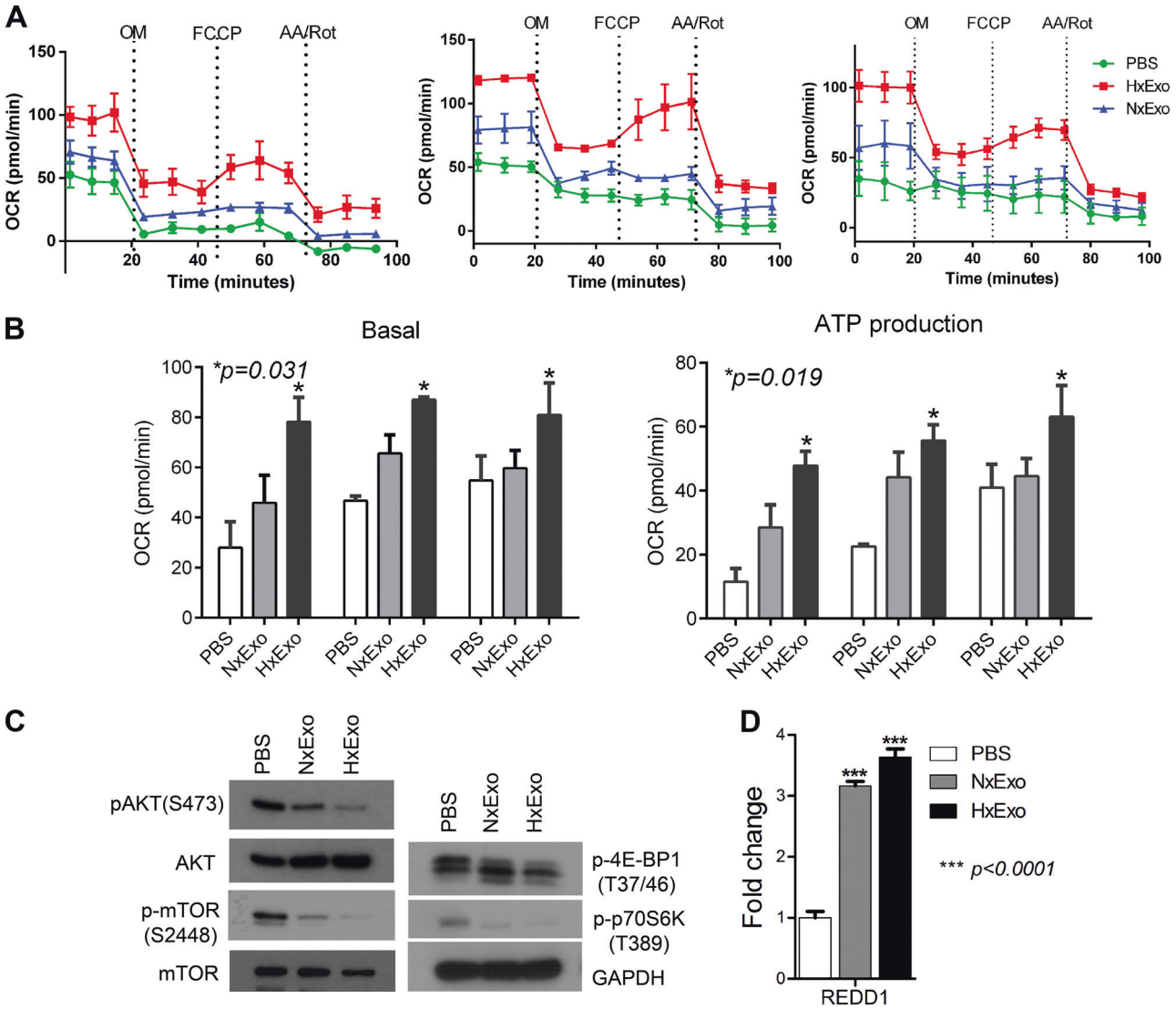

Fig. 4 Exosome-mediated enhancement of mitochondrial oxidative phosphorylation. **a** Oxygen consumption rate (OCR) of BMMs treated with NxExo, HxExo, or PBS control using mitochondrial stress test. OCR was tested in biological triplicates. **b** Basal respiration rate and ATP production were presented in biological triplicates. Paired *T*-test between PBS- and HxExo-treated BMMs was performed after combining three biological replicates. **c** Western bot analysis of phospho-Akt and phospho-mTOR as well as substrates p70S6K and 4E-BP1. **d** RT-qPCR analysis of REDD-1 expression level. Data represent the mean ± SEM of triplicate experiments, $***p < 0.0001$. NxExo normoxic exosomes, HxExo hypoxic exosomes

extremely lower than BMMs' gene expression changes. In addition, BMMs showed higher response to hypoxic condition when being co-cultured with B16-F0 cells by presenting more than 200-fold increase of *COX-2* and *IL-6* gene expression, while BMMs alone induce only ~4-fold changes under hypoxic culture (Fig. 6c). It implies that tumor-infiltrating immune cells, specifically macrophages, strongly react with secretory molecules derived from hypoxic tumor cells rather than hypoxic condition. Since an exosome has been demonstrated as a stable delivery vehicle of biomolecules, the exosome might take a key role in immune cell modulation in the tumor microenvironment. This specific M2-like polarization of exosome-treated BMMs, combined with our earlier observation of enhanced OXPHOS in these cells, strongly suggested that macrophages generated via this process might favor cancer progression. In order to test this, we cultured BMMs for 48 h in the presence of normoxic or hypoxic exosomes and then tested whether soluble factors released into the conditioned medium (CM) were capable of altering the tumor growth. When assessed by 3-(4,5-dimethylthiazol-2-yl)-2,5-diphenyltetrazolium bromide (MTT) assay, we observed that BMM-derived CM significantly increased B16-F0 tumor cell proliferation and viability, but growth rates were enhanced 3- to 4-fold more after transfer of CM generated by hypoxic exosome-treated macrophages (Fig. 6d).

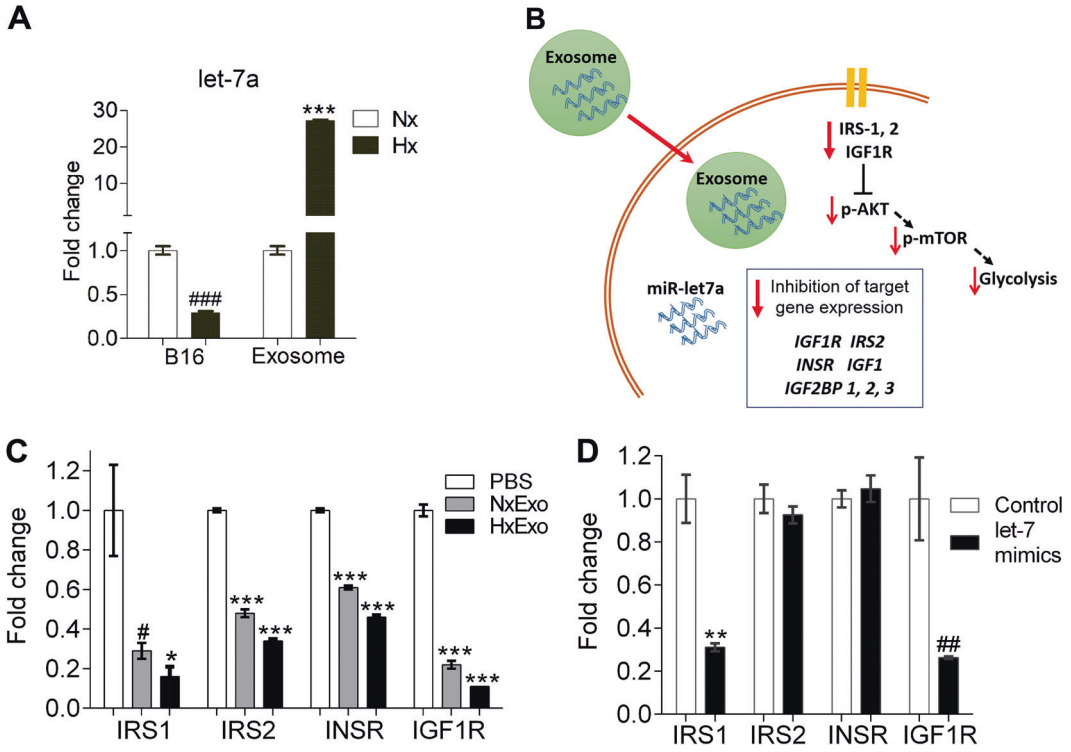

Fig. 5 Exosome-mediated transfer of miRNA let-7a to BMMs. **a** RT-qPCR analysis of let-7a miRNA levels in B16-F0 tumor cells and derivative exosomes. Data represent the mean ± SEM of triplicate experiments; ###$p = 0.0002$, ***$p < 0.0001$. **b** Proposed model for the role of exosomal let-7a miRNA in INS-AKT-mTOR pathway. Candidate let-7a miRNA target genes as predicted by TargetScan; insulin-like growth factor 1 receptor (*IGF1R*), insulin receptor (*INSR*), insulin receptor substrate-1 (*IRS-1*), *IRS-2*, insulin-like growth factor-1 (*IGF-1*), insulin-like growth factor 2 mRNA-binding protein 1 (*IGF2BP1*), *IGF2BP2*, and *IGF2BP3*. **c** RT-qPCR analysis of let-7 miRNA target gene expression in exosome-treated BMMs. Data represent the mean ± SEM of triplicate experiments; #$p = 0.0384$, *$p = 0.0234$. **d** RT-qPCR gene expression analysis of RAW264.7 macrophages after transfection with 50 nM of let-7a mimics. Data represent the mean ± SEM of triplicate; **$p = 0.0186$, ##$p = 0.0036$

Discussion

Exosomes are now widely recognized as critical mediators of tumor growth, angiogenesis, and metastasis, and have recently become a major focus of efforts to develop new cancer therapeutics. However, it remains unclear how exosome biology is modified by dynamic changes in the tumor microenvironment. Since tissue hypoxia is known to be a key regulator of tumor development [1, 44], we assessed how oxygen depletion influences tumor exosome release, protein composition, and effects on immune responses both in vitro and in vivo. Using a comprehensive proteomic approach, we observed that tumor exosomes are enriched in chemokines and growth factors that mediate monocyte/macrophage recruitment and host immunosuppression including CSF-1, CCL2, EMAP2, TGFβ, FTH, and FTL [25–28, 45, 46], and hypoxia substantially enhanced exosomal levels of these proteins 4–6-fold higher compared with vesicles generated under normal oxygen conditions (Fig. 2). These data suggest that exosomes released by hypoxic tumors may exert more potent effects on host immunity and alter the clinical course of human cancers.

In this study, the immunological effects of tumor exosomes were further investigated using bone marrow-derived myeloid cells, an origin of circulating and tissue-resident monocyte/macrophages [47]. We observed increased macrophage chemotaxis toward exosomes produced by hypoxic tumors relative to those released under standard culture conditions. In addition, hypoxic exosomes increased M2-like polarization of bone marrow-derived myeloid cells (F4/80^{+}CD206^{high} positive cells) without cytokine supplementation (Fig. 3c) and promoted change in macrophage immunometabolic profile to enhanced OXPHOS activity (Fig. 4) [48, 49]. These findings are consistent with earlier reports that M2-like macrophages can promote tumor proliferation and enhance the angiogenic potential of endothelial cells by favoring OXPHOS [50]. In parallel with these immunometabolic effects, hypoxic exosomes significantly increased the expression of M2-associated genes implicated in supporting cancer cell growth (*Arg-1, IL-6, COX2*, and *PGES)*, and CM obtained from these cells was capable of transferring an enhanced growth phenotype to fresh tumor cells that had not been directly exposed to exosomes.

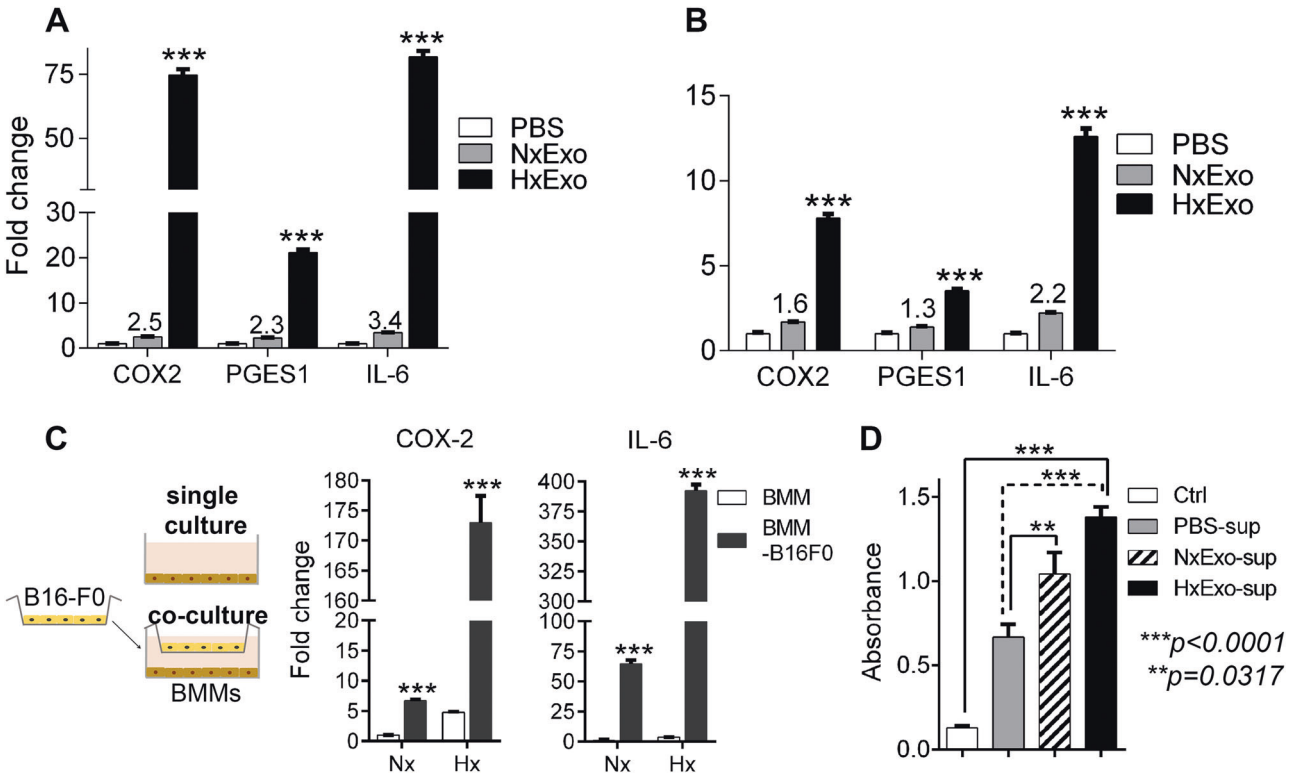

Fig. 6 Exosome-treated BMMs increased cancer cell growth. **a** RT-qPCR analysis of M2-associated genes, COX-2, PGES, and IL-6, in exosome-treated BMMs. Data represent the mean ± SEM of triplicate experiments; ***$p < 0.0001$. **b** RT-qPCR analysis of COX-2, PGES, and IL-6 in exosome-treated BMDCs. Data represent the mean ± SEM of triplicate experiments; ***$p < 0.0001$. **c** RT-qPCR analysis of COX-2 and IL-6 in BMM-B16-F0 co-culture system. Data represent the mean ± SEM of triplicate experiments; ***$p < 0.0001$. **d** B16-F0 tumor cell viability as assessed by MTT assay after 48 h culture with CM generated by BMMs exposed to normoxic exosomes (NxExo) or hypoxic exosomes (Hx-Exo) for the preceding 48 h (or PBS-only/normal medium control). Data represent the mean ± SEM of triplicate experiments

Our findings of exosome-mediated M2-like macrophage polarization were supported by hypoxic tumor-derived exosomes from various cancer cell lines including human melanoma, skin, and lung cancer cells. Tumor-derived exosomes, especially hypoxic exosomes, induced M2-like phenotypic changes from M0-like THP-1 cells, assessed by CD163+ marker and the expression of CCL13 (Supplementary Fig. 6), indicating the global role of tumor-derived exosomes in immune systems. Interestingly, tumor exosomes exhibited a potential role of hematopoietic stem cell differentiation as it increased F4/80^{+}CD135^{high} positive cell population in exosome-treated BMMs (Fig. 3d).

Exosome-enhanced OXPHOS activity in BMMs was associated with suppression of the mTOR pathway, suggesting a role of exosomes via inhibition of AKT-mTOR signaling pathway. In the present study, we identified let-7a miRNA, a known epigenetic tumor suppressor [51], as a candidate suppressor of insulin-mediated mTOR signaling pathway. Our data indicate that microenvironmental hypoxia was instead associated with decreased let-7a miRNA levels in cancer cells and a >20-fold increase in released exosomes, suggesting that this may represent a mechanism of expelling suppressive molecules from the tumor body. In turn, exosomal transfer of let-7a miRNA enhanced OXPHOS activity and M2-like polarization of infiltrating macrophages via downregulation of insulin-AKT-mTOR signaling pathway. While let-7a miRNA was enriched in hypoxic exosomes, the suppressive effects of exosomes on insulin signaling-related genes were significant in both normoxic and hypoxic exosome-treated cells. Therefore, further characterization of let-7a miRNA targets as well as hypoxic exosome-specific factors is necessary. These combined effects significantly increased tumor cell proliferation and survival in our assays in vitro, and are therefore also likely to exert major effects on cancer progression in human patients in vivo.

M2-like macrophage polarization and change in immunometabolic profile are now recognized as critical components of tumor progression and represent appealing targets for novel immunotherapies. In the current report, we provide a mechanistic link between the tumor microenvironment and M2-like polarization of infiltrating macrophages via exosomal transfer of immune mediators and suppressive miRNAs. Our proteomics data revealed that hypoxia exerts

profound effects on the composition of exosomal cargo, with many proteins displaying >2-fold change in abundance under these conditions. Since tumor hypoxia has long been associated with poor prognosis/therapy resistance, and exosome levels in serum are substantially increased in cancer, it is likely that hypoxia effects on exosome loading and release will significantly impact on disease progression in human patients. These findings also suggest that tumor exosome release into the circulatory system may represent a source of potential biomarkers for predicting clinical course and informing treatment strategies. Further studies will now be required to better define the role of hypoxic tumor exosomes in promoting therapy resistance in human patients, so that more effective immunotherapeutic approaches can be developed in future.

Materials and methods

Hollow fiber cell culture

Mouse melanoma B16-F0 cells and Raw 264.7 macrophage cells and human melanoma A375 cells, squamous skin carcinoma A431 cells, lung adenocarcinoma A549 cells, and monocytic THP-1 cells were purchased from American Type Culture Collection (ATCC, Manassas, VA, USA) and maintained in DMEM-high glucose media or RPMI 1640 (HyClone Laboratories, Logan, UT, USA) supplemented with 10% fetal bovine serum at 37 °C with 5% CO_2. All cell lines were tested free of mycoplasma contamination [52].

For exosome isolation, we used a hollow fiber culture (HFC) system to generate an in vivo-like 3D environment. All hollow fiber modules including Fibercell cartridges (#C2011) were purchased from Fibercell Systems Inc. (Frederick, MD, USA). Briefly, B16-F0, A375, A431, or A549 cells were inoculated into the extra-capillary space of each cartridge and allowed to attach to the fiber surface over 24 h. Cancer cells were maintained in DMEM supplemented with 5% Chemically Defined Medium for High Density cell culture (CDM-HD; Fibercell). CDM-HD, a chemically defined protein-free serum replacement, was used to avoid contamination of FBS-derived exosomes. After cell inoculation, the media reservoir was refreshed upon reaching 50% of initial glucose concentration, after which the cultures were subjected to either normoxia (Nx, 21% O_2) or hypoxia (Hx, 0.5% > O_2) for 24 h duration. Presence of oxygen was checked by Mitsubishi RT Anaero-Indicator (Thermo Fisher Scientific).

Exosome extraction, purification, and quantification

CM was collected from the hollow fiber cartridge's extracellular space after 24 h Nx or Hx culture, before being centrifuged at 1200 × *g*, 25 °C for 30 min to remove cell debris. The supernatants were then subjected to 300 kDa molecular weight cut off (MWCO) centrifugation at 4,000 × *g*, 4 °C to concentrate, then washed twice with PBS to remove residual media components such as sugars. The concentrated samples were subsequently centrifuged at 12,000 × *g*, 4 °C for 30 mins to eliminate microvesicles before pelleting the remaining exosomes via ultracentrifugation at 100,000 × g, 4 °C on a 5.5% sucrose pad for 15 h. Isolated exosomes were re-suspended in PBS and quantified prior to further analysis. Isolated exosomes were diluted in PBS and analyzed using the Nanosight NS300 System (Malvern Instruments, UK), which is equipped with a blue laser (405 nm). The Nanosight Tracking Analysis software was used to provide particle concentrations and size distribution profiles. For exosomal protein quantification, exosomes were mixed with equal volume of 10% SDS and boiled for 10 min to extract proteins from the membrane and inside the vesicles and then subsequently diluted 5-fold in PBS to dilute out SDS for BCA assay.

TMT labeling and liquid chromatography with tandem mass spectroscopy

A total of 250 µg denatured exosomes (generated either under Nx or Hx conditions) were loaded into 15% SDS-PAGE gels for electrophoresis at 100 V for 30 min. Each gel band was cut into small pieces and washed with 25 mM triethylammonium bicarbonate (TEAB) in 50% acetonitrile (ACN). The gel pieces were then dehydrated with 100% ACN and vacuum dried. Reduction was carried out using 5 mM Tris 2-carboxyethyl phosphine hydrochloride (TCEP) in 50 mM TEAB buffer at 60 °C for 60 min, followed by alkylation with 55 mM iodoacetamide (IAA) in 50 mM TEAB buffer at room temperature for 30 min. TCEP and IAA were removed by performing alternate washes with 50 mM TEAB buffer and 50 mM TEAB in 50% ACN. The gel pieces were then dehydrated and dried for a second time. The gel pieces were completely rehydrated with 10 ng/ml of sequencing-grade modified trypsin solution (Promega Corporation, Madison, WI, USA) in 100 mM TEAB (protein to trypsin ratio of 1:50) on ice and subsequently incubated at 37 °C for overnight digestion. Tryptic peptides were extracted using 50% ACN and 5% acetic acid before being dried by vacuum centrifugation (Eppendorf, USA). Labeling was performed using TMT reagent multiplex kits according to the manufacturer's protocol (Thermo Scientific, USA). The TMT-labeled

peptides were pooled and desalted using Sep-Pak C18 Vac cartridges (Waters, Milford, MA) before being vacuum-centrifuged to dry. Details of the labeling scheme used are provided in the Supplementary Data. The labeled samples were combined prior to fractionation on a Xbridge™ C18 column (4.6 × 250 mm, Waters, Milford, MA, USA) for subsequent analysis by LC-MS/MS.

The fractionated peptides were separated and analyzed using a Dionex Ultimate 3000 RSLCnano system coupled to a Q Exactive instrument (Thermo Fisher Scientific, MA, USA) as previously described [53]. The raw data were converted to Mascot generic file format using Proteome-Discoverer™ v1.4 software (PD, Thermo Scientific, San Jose, USA). The MS/MS spectra were deisotoped and deconvoluted using the MS2 spectrum processor node in PD. Protein identification and quantitation were performed by comparing MS/MS spectra against the Uniprot Human database (released on 7/25/2016, 70,849 sequences, 23,964,784 residues) using Mascot software version 2.41 (Matrix Sciences, London, UK). A threshold of maximum two missed trypsin cleavages was applied. Peptide precursor mass tolerances of 10 ppm and 0.02 Da were used during data search. TMT6 quantitation was used to measure the relative protein expression level. Fixed modifications were carbamidomethylation (+57.021 Da) of cysteine residues. Variable modifications were deamidation (+0.984 Da) of asparagine and glutamine residues, as well as oxidation (+15.995 Da) of methionine residues. All statistical analysis was performed using experimental triplicate. Reproducibility between the replicates was analyzed using linear regression analysis method. Statistical significance was determined by Student's *T* test. A frequency distribution analysis was used to determine the fold-change cutoff for relative protein abundance. Significantly changed proteins were determined by the volcano plot and used for the subsequent analysis (Supplementary Fig. S3).

Bone marrow cells isolation, differentiation, and exosome treatment

Eight-week-old male, B57CL/6NTac mice (InVivos, Pte. Ltd., Singapore) were used in all in vivo experiments. Bone marrow cells were extracted from mouse femurs and tibias via flushing with RPMI media through a 25 G needle. The samples were then passed through 40-μm cell strainers to obtain single cell suspension. Next, the cells were centrifuged at 300 × *g*, 25 °C for 10 min, re-suspended in red blood cell lysis buffer, and incubated for 10 min with gentle agitation every 60 s. The resultant cell suspensions were then pelleted via centrifugation and re-suspended in appropriate media/buffers as required for downstream applications. To obtain BMMs, isolated bone marrow cells were cultured for 7 days in RPMI medium supplemented with 10% FBS and M-CSF (25 ng/ml, BioLegend, San Diego, CA, USA). For generation of BMDCs, isolated bone marrow cells were cultured for 7 days in RPMI medium supplemented with 10% FBS and GM-CSF (20 ng/ml, BioLegend).

To examine the exosome-mediated macrophage polarization, 5 μg/ml of normoxic or hypoxic exosomes were treated on BMMs supplemented with 10% exosome-free FBS (Gibco exosome-depleted FBS, Thermo Fisher Scientific) and M-CSF (25 ng/ml) for 2 days. IL-4 (20 ng/ml, BioLegend) was used for M2-type macrophage polarization (Supplementary Fig. S5). Exosome-treated cells were subjected to western blot analysis, RT-qPCR, and FACS analysis.

THP-1 cell differentiation and exosome treatment

Differentiation of THP-1 monocytic cells into a macrophage-like (M0) phenotype was done by treatment with 20 ng/ml phorbol-12-myristate-13-acetate (PMA; Sigma-Aldrich) for 24 h in 5% FBS–RPMI media followed by resting in 10% FBS–RPMI control media for 24 h. Following treatment, differentiated cells were washed twice with PBS before being dissociated with cell dissociation solution (Invitrogen) and seeded onto 5-cm dish and 5 μg/ml of exosomes in 10% exosome-free FBS–RPMI media were treated for 48 h.

Macrophage invasion assay

Mouse RAW 264.7 macrophages were seeded onto Transwell® inserts coated with Matrigel and cultured in a 24-well plate with 10 μg of normoxic or hypoxic exosome-containing medium (1% exosome-free FBS-DMEM) in lower chamber. Cell invasion in response to normoxic or hypoxic exosomes was monitored for 24 h and migrated cells on the bottom membrane were fixed, visualized, and quantitated by crystal violet staining.

Western blot analysis

BMMs were treated with exosomes as described above. Cells were washed in ice-cold PBS and lysed in modified RIPA buffer (50 mM Tris–HCl, 150 mM NaCl, 1% NP-40, pH 8.0, 1× protease inhibitor cocktail, phosphatase inhibitors). Lysates were clarified by centrifugation (16,000 × g, 30 min) and subjected to western blotting using the indicated primary antibodies at 1:1000 dilution. Protein–antibody conjugates were visualized using a chemiluminescence detection kit (Thermo Fisher Scientific). Antibodies against exosomal markers, Alix, CD63, and TSG101, were obtained from Santa Cruz Biotechnology (Santa Cruz, USA). Antibodies to HIF-1α, STAT1,

pSTAT1 Y701, STAT6, pSTAT6 Y641, mTOR, p-mTOR S2448, pS6K T398, p4E-BP T37/46, AKT, and pAKT S473 were purchased from Cell Signaling Technologies (Danvers, MA, USA). Actin, tubulin, and GAPDH antibodies were obtained from Millipore (Billerica, MA).

Total RNA and miRNA extraction and RT-qPCR

BMMs were treated with exosomes as described above and subjected to total RNA or miRNA extraction. Total RNA extraction was performed using Nucleospin RNA kits (MACHEREY-NAGEL GmbH & Co.) according to the manufacturer's protocol. RT-qPCR was performed using a CFX96 Real-Time PCR Detection System (Bio-Rad) with KAPA SYBR® FAST qPCR Master Mix. Actin or 18 s RNA were used as internal controls. To detect the level of miR-let-7a, we used mirVana^{TM} miRNA isolation kit (Invitrogen) to isolate miRNA according to the manufacturer's protocol and subsequently, miRNA was reverse transcribed using miRCURY LNA^{TM} Universal cDNA Synthesis Kit (Exiqon, Denmark). Synthetic UniSp6, a spike-in control, was used to monitor the efficiency of the RT reaction. The primers for U6 and miR-let-7a were obtained from Exiqon.

We transfected 50 nM of mse-let-7a-mimics (UGAGGUAGUAGGUUGUAUAG) to mouse Raw264.7 cells using jetPEI-macrophage transfection reagent (PolyPlus Transfection, Illkirch, France) and tested for expression of insulin signaling molecules by RT-qPCR after 24 h. The primer sequences used for real-time PCR are provided in the Supplementary Information (Supplementary Table S5).

Leukocyte infiltration assay

Eight-week-old male, B57CL/6NTac mice were purchased from InVivos and randomly assigned to different treating groups for leukocyte infiltration assay. A total of 1×10^6 B16-F0 tumor cells in growth factor-reduced Matrigel were premixed with either normoxic or hypoxic exosomes (50 μg) and then administered via s.c. injection into the back of B57CL/6NTac mice ($n = 6$ per group). Tumor sizes were then assessed daily by routine caliper measurement. Mice were euthanized when the tumor size exceeded 1.5 cm diameter, as per protocol guidelines. The tumors were then excised, finely minced, and enzymatically dissociated using collagenase D (2 mg/ml) and DNase I (20 μg/ml) for 30 min at 37 °C to obtain single cell suspensions. Isolated cell suspension was subjected to antibody staining with anti-F4/80-FITC and anti-CD206-PE (Miltenyi Biotech GmbH, Bergisch Gladbach, Germany) for FACS analysis. All animal studies were approved by an Institutional Animal Care and Use Committee (IACUC, ARF-SBS/NIE-A0286) and were performed in accordance with approved guidelines and regulations of the Animal Facility Center of the School of Biological Sciences, Nanyang Technological University, Singapore.

Flow cytometric analysis for exosome-mediated BMM polarization

We used three different batches of exosome samples to examine the effects and reproducibility of exosome treatment on BMM polarization. Normoxic or hypoxic exosomes were treated as described above and further stained with Fluorochrome-conjugated antibodies, CD11c-APC, MHCII-PerCP-Vio700^{TM}, F4/80-FITC, CD3-PerCP-Vio®700, CD25-PE, CD8a-APC, CD4-FITC, and CD135-PerCP-Vio700^{TM} (Miltenyi Biotech, Bergisch Gladbach, Germany) and CD206-PE (Biolegend). M2-type polarization of THP-1 cells was detected with CD163-PE (Biolegend). Labeled cells were analyzed using a FACSCalibur flow cytometer (BD, San Jose, CA) and FlowJo software (Tree Star Inc., Oregon, USA).

Metabolic assays

OCR of BMMs was measured with a XF24 extracellular flux analyzer (Seahorse Bioscience). Briefly, BMMs underwent the same exosome treatment for polarization and 4×10^4 exosome-treated BMMs cells/well were seeded in a XF-24 cell culture microplate, a part of Seahorse XF24 FluxPak (Seahorse Bioscience, Agilent Technologies, Santa Clara, CA, USA), and OCR measurements were normalized to cell number. Cells were initially plated in XF Seahorse media with both glucose and glutamine in mitochondrial stress test using the following concentrations of injected compounds, as according to the manufacturer's standard protocol (XF cell mito stress test kit, Seahorse Bioscience): OM, 1 μM; ROT, 0.75 μM; electron transport chain accelerator *p*-trifluoromethoxy carbonyl cyanide phenyl hydrazine (FCCP), 0.5 μM; AA, 1.5 μM. OCR test was independently performed with three different batches of exosome samples to test the effect of exosomes on metabolic changes.

Statistical analysis

Statistical analyses were performed using SPSS18 software (v18.0; SPSS, Chicago, IL, USA). Differences between groups were assessed by Student's *t*-test and $p < 0.05$ was considered as significant.

Acknowledgements This work is in part supported by grants from the Singapore Ministry of Education (MOE2014-T2-2-043, MOE2016-T2-2-018, and MOE2016-T3-1-003) and the National Medical Research Council of Singapore (NMRC-OF-IRG-0003-2016).

Author contributions JEP designed and performed the experiments, analyzed the data, and wrote the paper; BD performed the exosome TMT proteomics experiments and analyzed the data; SWT and NG performed animal experiments; CFT performed exosome preparation and analysis; and JKL, KWY, OLK, and JPT contributed to reagents and discussion; SSK conceived, designed, supervised the project, and revised the manuscript. All co-authors contributed to the revision of the manuscript.

Compliance with ethical standards

Conflict of interest The authors declare that they have no conflict of interest.

Publisher's note: Springer Nature remains neutral with regard to jurisdictional claims in published maps and institutional affiliations.

References

1. Park JE, Tan HS, Datta A, Lai RC, Zhang H, Meng W, et al. Hypoxic tumor cell modulates its microenvironment to enhance angiogenic and metastatic potential by secretion of proteins and exosomes. Mol Cell Proteom. 2010;9:1085–99.
2. Wilson WR, Hay MP. Targeting hypoxia in cancer therapy. Nat Rev Cancer. 2011;11:393–410.
3. Colombo M, Raposo G, Théry C. Biogenesis, secretion, and intercellular interactions of exosomes and other extracellular vesicles. Annu Rev Cell Dev Biol. 2014;30:255–89.
4. De Toro J, Herschlik L, Waldner C, Mongini C. Emerging roles of exosomes in normal and pathological conditions: new insights for diagnosis and therapeutic applications. Front Immunol. 2015;4:203.
5. Simons M, Raposo G. Exosomes—vesicular carriers for intercellular communication. Curr Opin Cell Biol. 2009;21:575–81.
6. Liu Y, Gu Y, Han Y, Zhang Q, Jiang Z, Zhang X, et al. Tumor exosomal rnas promote lung pre-metastatic niche formation by activating alveolar epithelial TLR3 to recruit neutrophils. Cancer Cell. 2016;30:243–56.
7. Peinado H, Alečković M, Lavotshkin S, Matei I, Costa-Silva B, Moreno-Bueno G, et al. Melanoma exosomes educate bone marrow progenitor cells toward a pro-metastatic phenotype through MET. Nat Med. 2012;18:883–91.
8. Wu L, Zhang X, Zhang B, Shi H, Yuan X, Sun Y, et al. Exosomes derived from gastric cancer cells activate NF-κB pathway in macrophages to promote cancer progression. Tumor Biol. 2016;37:12169–80.
9. Boelens Mirjam C, Wu Tony J, Nabet Barzin Y, Xu B, Qiu Y, Yoon T, et al. Exosome transfer from stromal to breast cancer cells regulates therapy resistance pathways. Cell. 2014;159:499–513.
10. Hoffman RM. Stromal-cell and cancer-cell exosomes leading the metastatic exodus for the promised niche. Breast Cancer Res. 2013;15:310.
11. Robbins PD, Morelli AE. Regulation of immune responses by extracellular vesicles. Nat Rev Immunol. 2014;14:195–208.
12. Viaud S, Terme M, Flament C, Taieb J, André F, Novault S, et al. Dendritic cell-derived exosomes promote natural killer cell activation and proliferation: a role for NKG2D ligands and IL-15Rα. PLoS ONE. 2009;4:e4942.
13. Bretz NP, Ridinger J, Rupp A-K, Rimbach K, Keller S, Rupp C, et al. Body fluid exosomes promote secretion of inflammatory cytokines in monocytic cells via toll-like receptor signaling. J Biol Chem. 2013;288:36691–702.
14. Whiteside TL. Exosomes and tumor-mediated immune suppression. J Clin Invest. 2016;126:1216–23.
15. Espinoza JL, Takami A, Yoshioka K, Nakata K, Sato T, Kasahara Y, et al. Human microRNA-1245 down-regulates the NKG2D receptor in natural killer cells and impairs NKG2D-mediated functions. Haematologica. 2012;97:1295–303.
16. Zhou J, Wang S, Sun K, Chng W-J. The emerging roles of exosomes in leukemogeneis. Oncotarget. 2016;7:50698–707.
17. Lobb RJ, Lima LG, Möller A. Exosomes: key mediators of metastasis and pre-metastatic niche formation. Semin Cell Dev Biol. 2017;67:3–10.
18. Kucharzewska P, Belting M. Emerging roles of extracellular vesicles in the adaptive response of tumour cells to microenvironmental stress. J Extracell Vesicles. 2013;2:1–10.
19. Villarroya-Beltri C, Baixauli F, Gutierrez-Vazquez C, Sanchez-Madrid F, Mittelbrunn M. Sorting it out: regulation of exosome loading. Semin Cancer Biol. 2014;28:3–13.
20. Wargo JA, Reddy SM, Reuben A, Sharma P. Monitoring immune responses in the tumor microenvironment. Curr Opin Immunol. 2016;41:23–31.
21. Storm MP, Sorrell I, Shipley R, Regan S, Luetchford KA, Sathish J, et al. Hollow fiber bioreactors for in vivo-like mammalian tissue culture. J Vis Exp. 2016:53431.
22. Thompson A, Schäfer J, Kuhn K, Kienle S, Schwarz J, Schmidt G, et al. Tandem mass tags: a novel quantification strategy for comparative analysis of complex protein mixtures by MS/MS. Anal Chem. 2003;75:1895–904.
23. Semenza GL. HIF-1 and tumor progression: pathophysiology and therapeutics. Trends Mol Med. 2002;8:S62–7.
24. Zhu Q, Wong AK, Krishnan A, Aure MR, Tadych A, Zhang R, et al. Targeted exploration and analysis of large cross-platform human transcriptomic compendia. Nat Methods. 2015;12:211–4.
25. Lin EY, Nguyen AV, Russell RG, Pollard JW. Colony-stimulating factor 1 promotes progression of mammary tumors to malignancy. J Exp Med. 2001;193:727–40.
26. Qian B-Z, Li J, Zhang H, Kitamura T, Zhang J, Campion LR, et al. CCL2 recruits inflammatory monocytes to facilitate breast tumor metastasis. Nature. 2011;475:222–5.
27. Gray CP, Arosio P, Hersey P. Association of increased levels of heavy-chain ferritin with increased CD4+CD25+regulatory T-cell levels in patients with melanoma. Clin Cancer Res. 2003;9:2551–9.
28. Marie JC, Letterio JJ, Gavin M, Rudensky AY. TGF-β1 maintains suppressor function and Foxp3 expression in CD4+CD25+regulatory T cells. J Exp Med. 2005;201:1061–7.
29. Kumar V, Patel S, Tcyganov E, Gabrilovich DI. The nature of myeloid-derived suppressor cells in the tumor microenvironment. Trends Immunol. 2016;37:208–20.
30. Ugel S, De Sanctis F, Mandruzzato S, Bronte V. Tumor-induced myeloid deviation: when myeloid-derived suppressor cells meet tumor-associated macrophages. J Clin Invest. 2015;125:3365–76.
31. Green CE, Liu T, Montel V, Hsiao G, Lester RD, Subramaniam S, et al. Chemoattractant signaling between tumor cells and macrophages regulates cancer cell migration, metastasis and neovascularization. PLoS ONE. 2009;4:e6713.
32. Damuzzo V, Pinton L, Desantis G, Solito S, Marigo I, Bronte V, et al. Complexity and challenges in defining myeloid-derived suppressor cells. Cytometry B Clin Cytom. 2015;88:77–91.
33. Kikushige Y, Yoshimoto G, Miyamoto T, Iino T, Mori Y, Iwasaki H, et al. Human Flt3 is expressed at the hematopoietic stem cell and the granulocyte/macrophage progenitor stages to maintain cell survival. J Immunol. 2008;180:7358–67.
34. Geeraerts X, Bolli E, Fendt S-M, Van Ginderachter JA. Macrophage metabolism as therapeutic target for cancer, atherosclerosis, and obesity. Front Immunol. 2017;8:289.

35. Mosser DM, Edwards JP. Exploring the full spectrum of macrophage activation. Nat Rev Immunol. 2008;8:958–69.
36. Roszer T. Understanding the mysterious M2 macrophage through activation markers and effector mechanisms. Mediators Inflamm. 2015;2015:816460.
37. Genin M, Clement F, Fattaccioli A, Raes M, Michiels C. M1 and M2 macrophages derived from THP-1 cells differentially modulate the response of cancer cells to etoposide. BMC Cancer. 2015;15:577–577.
38. Hu JM, Liu K, Liu JH, Jiang XL, Wang XL, Chen YZ, et al. CD163 as a marker of M2 macrophage, contribute to predicte aggressiveness and prognosis of Kazakh esophageal squamous cell carcinoma. Oncotarget. 2017;8:21526–38.
39. Sudan B, Wacker MA, Wilson ME, Graff JW. A systematic approach to identify markers of distinctly activated human macrophages. Front Immunol. 2015;6:253.
40. Biswas Subhra K. Metabolic reprogramming of immune cells in cancer progression. Immunity. 2015;43:435–49.
41. Otero-Albiol D, Felipe-Abrio B. MicroRNA regulating metabolic reprogramming in tumor cells: new tumor markers. Cancer Transl Med. 2016;2:175–81.
42. Zhu H, Shyh-Chang N, Segrè Ayellet V, Shinoda G, Shah Samar P, Einhorn William S, et al. The Lin28/let-7 axis regulates glucose metabolism. Cell. 2011;147:81–94.
43. Lewis BP, Burge CB, Bartel DP. Conserved seed pairing, often flanked by adenosines, indicates that thousands of human genes are microRNA targets. Cell. 2004;120:15–20.
44. Finger EC, Giaccia AJ. Hypoxia, inflammation, and the tumor microenvironment in metastatic disease. Cancer Metastasis Rev. 2010;29:285–93.
45. Kao J, Houck K, Fan Y, Haehnel I, Libutti SK, Kayton ML, et al. Characterization of a novel tumor-derived cytokine. Endothelial-monocyte activating polypeptide II. J Biol Chem. 1994;269:25106–19.
46. Kore RA, Edmondson JL, Jenkins SV, Jamshidi-Parsian A, Dings RPM, Reyna NS, et al. Hypoxia-derived exosomes induce putative altered pathways in biosynthesis and ion regulatory channels in glioblastoma cells. Biochem Biophys Rep. 2018;14:104–13.
47. Elliott LA, Doherty GA, Sheahan K, Ryan EJ. Human tumor-infiltrating myeloid cells: phenotypic and functional diversity. Front Immunol. 2017;8:86.
48. Galván-Peña S, O'Neill LAJ. Metabolic reprograming in macrophage polarization. Front Immunol. 2014;5:420.
49. O'Neill LAJ, Pearce EJ. Immunometabolism governs dendritic cell and macrophage function. J Exp Med. 2016;213:15–23.
50. Wenes M, Shang M, Di Matteo M, Goveia J, Martín-Pérez R, Serneels J, et al. Macrophage metabolism controls tumor blood vessel morphogenesis and metastasis. Cell Metab. 2016;24:701–15.
51. Jérôme T, Laurie P, Louis B, Pierre C. Enjoy the silence: the story of let-7 microRNA and cancer. Curr Genomics. 2007;8:229–33.
52. Young L, Sung J, Stacey G, Masters JR. Detection of mycoplasma in cell cultures. Nat Protoc. 2010;5:929.
53. Park JE, Sun Y, Lim SK, Tam JP, Dekker M, Chen H, et al. Dietary phytochemical PEITC restricts tumor development via modulation of epigenetic writers and erasers. Sci Rep. 2017;7:40569.
54. Hume DA, MacDonald KPA. Therapeutic applications of macrophage colony-stimulating factor-1 (CSF-1) and antagonists of CSF-1 receptor (CSF-1R) signaling. Blood. 2012;119:1810–20.
55. Murdoch C, Giannoudis A, Lewis CE. Mechanisms regulating the recruitment of macrophages into hypoxic areas of tumors and other ischemic tissues. Blood. 2004;104:2224–34.
56. Nielsen SR, Schmid MC. Macrophages as key drivers of cancer progression and metastasis. Mediators Inflamm. 2017;2017:11.
57. Li M, Knight DA, A Snyder L, Smyth MJ, Stewart TJ. A role for CCL2 in both tumor progression and immunosurveillance. Oncoimmunology. 2013;2:e25474.
58. Lee DD, Lal CV, Persad EA, Lowe C-W, Schwarz AM, Awasthi N, et al. Endothelial monocyte-activating polypeptide II mediates macrophage migration in the development of hyperoxia-induced lung disease of prematurity. Am J Respir Cell Mol Biol. 2016;55:602–12.
59. Jia W, Kidoya H, Yamakawa D, Naito H, Takakura N. Galectin-3 accelerates M2 macrophage infiltration and angiogenesis in tumors. Am J Pathol. 2013;182:1821–31.
60. Alkhateeb AA, Han B, Connor JR. Ferritin stimulates breast cancer cells through an iron-independent mechanism and is localized within tumor-associated macrophages. Breast Cancer Res Treat. 2013;137:733–44.
61. Gray CP, Arosio P, Hersey P. Heavy chain ferritin activates regulatory T cells by induction of changes in dendritic cells. Blood. 2002;99:3326–34.
62. Alkhateeb AA, Connor JR. The significance of ferritin in cancer: anti-oxidation, inflammation and tumorigenesis. Biochim Biophys Acta. 2013;1836:245–54.
63. Jezequel P, Campion L, Spyratos F, Loussouarn D, Campone M, Guerin-Charbonnel C, et al. Validation of tumor-associated macrophage ferritin light chain as a prognostic biomarker in node-negative breast cancer tumors: a multicentric 2004 national PHRC study. Int J Cancer. 2012;131:426–37.
64. Wu T, Li Y, Liu B, Zhang S, Wu L, Zhu X, et al. Expression of ferritin light chain (FTL) Is elevated in glioblastoma, and FTL silencing inhibits glioblastoma cell proliferation via the GADD45/JNK pathway. PLoS ONE. 2016;11:e0149361.
65. Bellomo C, Caja L, Moustakas A. Transforming growth factor β as regulator of cancer stemness and metastasis. Br J Cancer. 2016;115:761.
66. Lebrun J-J. The dual role of TGF in human cancer: from tumor suppression to cancer metastasis. ISRN Mol Biol. 2012;2012:28.
67. Tauriello DVF, Palomo-Ponce S, Stork D, Berenguer-Llergo A, Badia-Ramentol J, Iglesias M, et al. TGFβ drives immune evasion in genetically reconstituted colon cancer metastasis. Nature. 2018;554:538.
68. Chen X, Wang S, Wu N, Yang CS. Leukotriene A4 hydrolase as a target for cancer prevention and therapy. Curr Cancer Drug Targets. 2004;4:267–83.
69. Vo TTL, Jang WJ, Jeong CH. Leukotriene A4 hydrolase: an emerging target of natural products for cancer chemoprevention and chemotherapy. Ann N Y Acad Sci. 2018;1431:3–13.
70. Balogh KN, Templeton DJ, Cross JV. Macrophage Migration Inhibitory Factor protects cancer cells from immunogenic cell death and impairs anti-tumor immune responses. PLoS ONE. 2018;13:e0197702.
71. Kindt N, Journe F, Laurent G, Saussez S. Involvement of macrophage migration inhibitory factor in cancer and novel therapeutic targets. Oncol Lett. 2016;12:2247–53.
72. Chen SC, Kung ML, Hu TH, Chen HY, Wu JC, Kuo HM, et al. Hepatoma-derived growth factor regulates breast cancer cell invasion by modulating epithelial--mesenchymal transition. J Pathol. 2012;228:158–69.
73. Gialeli C, Theocharis AD, Karamanos NK. Roles of matrix metalloproteinases in cancer progression and their pharmacological targeting. FEBS J. 2011;278:16–27.

74. Wang D, Zhang S, Chen F. High expression of PLOD1 drives tumorigenesis and affects clinical outcome in gastrointestinal carcinoma. Genet Test Mol Biomarkers. 2018;22:366–73.
75. Gilkes DM, Bajpai S, Wong CC, Chaturvedi P, Hubbi ME, Wirtz D, et al. Procollagen lysyl hydroxylase 2 is essential for hypoxia-induced breast cancer metastasis. Mol Cancer Res. 2013;11:456–66.
76. Mogami T, Yokota N, Asai-Sato M, Yamada R, Koizume S, Sakuma Y, et al. Annexin A4 is involved in proliferation, chemoresistance and migration and invasion in ovarian clear cell adenocarcinoma cells. PLoS ONE. 2013;8:e80359.
77. Winter J, Diederichs S. Argonaute proteins regulate microRNA stability: Increased microRNA abundance by Argonaute proteins is due to microRNA stabilization. RNA Biol. 2011;8:1149–57.
78. Dueck A, Ziegler C, Eichner A, Berezikov E, Meister G. microRNAs associated with the different human Argonaute proteins. Nucleic Acids Res. 2012;40:9850–62.
79. Leca J, Martinez S, Lac S, Nigri J, Secq V, Rubis M, et al. Cancer-associated fibroblast-derived annexin A6+extracellular vesicles support pancreatic cancer aggressiveness. J Clin Invest. 2016;126:4140–56.
80. Qi H, Liu S, Guo C, Wang J, Greenaway FT, Sun M-Z. Role of annexin A6 in cancer. Oncol Lett. 2015;10:1947–52.